

The future evolution of the Southern Ocean CO₂ sink

by Nicole S. Lovenduski^{1,2} and Takamitsu Ito¹

ABSTRACT

We investigate the impact of century-scale climate changes on the Southern Ocean CO₂ sink using an idealized ocean general circulation and biogeochemical model. The simulations are executed under both constant and changing wind stress, freshwater fluxes, and atmospheric $p\text{CO}_2$, so as to separately analyze changes in natural and anthropogenic CO₂ fluxes under increasing wind stress and stratification. We find that the Southern Ocean sink for total contemporary CO₂ is weaker under increased wind stress and stratification by 2100, relative to a control run with no change in physical forcing, although the results are sensitive to the magnitude of the imposed physical changes and the rate of increase of atmospheric $p\text{CO}_2$. The air-sea fluxes of both natural and anthropogenic CO₂ are sensitive to the surface concentration of dissolved inorganic carbon (DIC) which responds to perturbations in wind stress and stratification differently. Spatially averaged surface DIC scales linearly with wind stress, primarily driven by changes in the Ekman transport. In contrast, changes in the stratification cause non-linear and more complex responses in spatially averaged surface DIC, involving shifts in the location of isopycnal outcrop for deep and thermocline waters. Thus, it is likely that both wind stress and stratification changes will influence the strength of the Southern Ocean CO₂ sink in the coming century.

1. Introduction

Oceanic models (Lovenduski *et al.*, 2008), atmospheric data (Le Quéré *et al.*, 2007), and oceanic observations (Metzl, 2009) indicate that the Southern Ocean sink for atmospheric CO₂ has substantially weakened in the last few decades, relative to the expected sink from rising atmospheric CO₂ and fixed physical climate. It has been suggested that the primary cause of the sink reduction is a trend in the position and intensity of the Southern Hemisphere westerly winds and the subsequent increase in the upwelling and equatorward transport of CO₂-rich waters (Le Quéré *et al.*, 2007; Lovenduski *et al.*, 2008). As simulations of future climate from coupled models consistently find a trend toward stronger, poleward shifted winds over the Southern Ocean during the next century (Miller *et al.*, 2006; Meehl *et al.*, 2007), it is possible that a further weakening of the Southern Ocean CO₂ sink will occur.

1. Department of Atmospheric Science, Colorado State University, Fort Collins, Colorado, 80523, U.S.A.

2. Present address: Department of Atmospheric and Oceanic Sciences and Institute of Arctic and Alpine Research, University of Colorado at Boulder, Boulder, Colorado, 80309, U.S.A. *email:* nicole.lovenduski@colorado.edu

The impact of future secular trends in Southern Hemisphere wind stress on Southern Ocean air-sea CO₂ flux are predicted to be accompanied by changes in climate-driven effects, such as the stratification of the global oceans (Fung *et al.*, 2005). The Southern Ocean in particular will likely experience a large increase in stratification due to enhanced melting of land and sea ice, warmer surface ocean temperatures, and enhanced precipitation at high latitudes (Manabe and Stouffer, 1993; Sarmiento *et al.*, 1998; Hirst, 1999; Sarmiento *et al.*, 2004b; Bitz *et al.*, 2006). A stratification change of this type can simultaneously reduce the upward flux of natural CO₂ (Toggweiler, 1999) and the downward flux of anthropogenic CO₂ (Sarmiento *et al.*, 1998) in the Southern Ocean, making it difficult to predict the impact of stratification on the total CO₂ sink.

Accurate predictions for the future evolution of the Southern Ocean CO₂ sink therefore require understanding how both wind stress and stratification impact carbon cycling and CO₂ exchange in this region. It has been suggested by Matear and Lenton (2008) that, over the past 5 decades, increased wind stress and increased stratification of the Southern Ocean have led to an equal and opposite CO₂ flux response. Furthermore, Matear and Lenton (2008) find that changes in Southern Ocean natural CO₂ exchange have always been countered by much smaller changes in anthropogenic CO₂ uptake over this time period. It is of critical importance to know if these compensatory processes will continue to operate in a future characterized by increased atmospheric CO₂ concentrations, when wind stress and stratification changes are likely to continue.

Unfortunately, predictions for the future evolution of the Southern Ocean CO₂ sink are plagued by uncertainties in the estimated future state of the atmosphere and the strength of climate feedback processes. While it is well-accepted that wind stress and stratification will somewhat increase in this region, the magnitude of the changes in these quantities differs substantially among the general circulation models in the IPCC AR4 (W. Lefebvre, pers. comm., 2008; Meehl *et al.*, 2007), making it difficult to accurately represent the future state of CO₂ fluxes in such models. One possible route to characterizing future behavior is by performing a suite of sensitivity studies in a simplified framework, in order to better understand the mechanisms leading to change.

Here, we use an idealized model to explore the possible future evolution of the Southern Ocean natural and anthropogenic carbon cycles under both enhanced wind stress and increased stratification. We simulate the ocean carbon cycle using an ocean general circulation model with a simplified geometry and biogeochemistry. We then probe the model with various configurations of atmospheric forcing and CO₂ boundary conditions to separately examine these processes in the most simplified and theoretical manner.

2. Model configuration and experiments

We investigate the impact of changes in wind stress and stratification on the Southern Ocean CO₂ sink using a sector version of the MIT ocean general circulation and biogeochemical model (Ito and Follows, 2005). The model is configured with an idealized

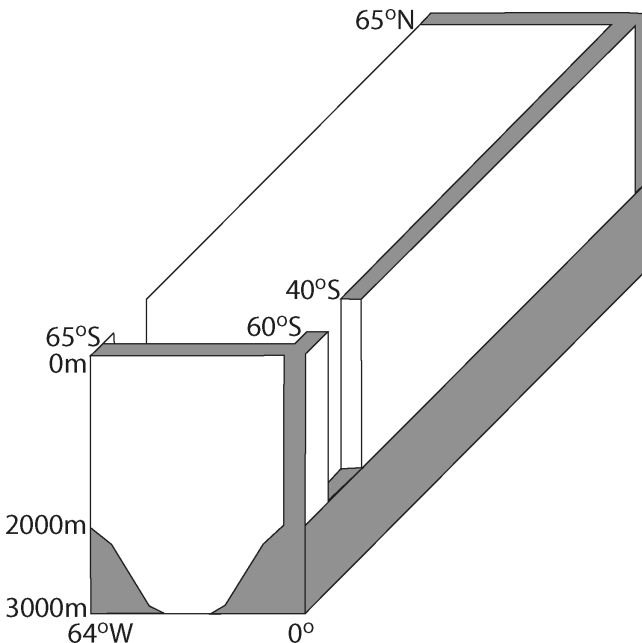


Figure 1. Configuration of the sector model used in the study.

bathymetry, such that it represents an interhemispheric, rectangular ocean basin with an open channel in the Southern Hemisphere (Fig. 1). A periodic boundary condition is applied to this open channel, simulating the flow of the Antarctic Circumpolar Current, which extends to 2000 m depth. The full model domain extends from 65°N to 65°S, and to a flat bottom at 3000 m. We run the model with a horizontal resolution of 2° and 30 vertical layers of varying thickness. Eddies are parameterized according to the Gent and McWilliams (1990) scheme with a constant isopycnal thickness diffusivity. The small domain size and coarse resolution allow the model to be run at a very low computational cost, making it ideal for use in sensitivity studies.

The physical model is forced with a sinusoidal zonal wind stress profile, and surface temperature and salinity are restored on a 1 month timescale to prescribed sinusoidal profiles, which are broadly consistent with the modern ocean climatology. There is no seasonal variation in these forcing profiles, and no sea ice component in the model.

The biogeochemical component of this model is also highly idealized. It consists of 5 passive tracers: dissolved inorganic carbon (DIC), alkalinity, dissolved oxygen, phosphate, and dissolved organic phosphorous. These tracers evolve with physical transport, biological uptake and remineralization, and air-sea gas exchange. Biological uptake is parameterized using Michaelis-Menton kinetics, with a uniform, constant maximum uptake rate and half-saturation coefficient for all simulations. Air-sea CO₂ exchange is parameterized according to Wanninkhof (1992), with an evolving ocean $p\text{CO}_2$ and prescribed atmospheric $p\text{CO}_2$.

Table 1. Sensitivity experiments conducted with the sector model.

simulation	wind magnitude	wind position	freshwater	CO ₂ 278	CO ₂ 450	CO ₂ 900	fixed export
1				x			
2					x		
3						x	
4	x			x			
5	x				x		
6	x					x	
7	x			x			x
8		x		x			
9			x	x			
10			x		x		
11			x			x	
12			x	x			x
13	x		x	x			
14	x		x		x		
15	x		x			x	

The model is initialized with uniform distributions of all tracers and spun up for a period of 3000 years under constant physical forcing and restoring profiles and an atmospheric $p\text{CO}_2$ boundary condition of 278 ppmv. This long integration period allows ocean CO₂ to come into equilibrium with the atmosphere, and there is no measurable drift in the modeled, globally integrated air-sea flux of CO₂ (not shown).

Following the spinup, we conduct three separate sets of simulations with different atmospheric $p\text{CO}_2$ boundary conditions (Table 1, Fig. 2a). In the first, atmospheric $p\text{CO}_2$ is set to the constant, pre-industrial spin-up value of 278 ppmv. In the second and third, this boundary condition is increased as piecewise linear fits to the measured and reconstructed atmospheric $p\text{CO}_2$ from 1765 until 2000, and from 2000 until 2100, with stabilized values after 2100 of 450 ppmv and 900 ppmv, respectively. These endpoints were chosen because they represent an extreme range of atmospheric CO₂ concentrations in 2100, as predicted by various economic development scenarios. From the first set of simulations, we obtain information about the fluxes of natural CO₂, whereas from the second and third set, we obtain information about the fluxes of contemporary CO₂. The difference between the fluxes of contemporary and natural CO₂ is considered to be the fluxes of anthropogenic CO₂ (Lovenduski *et al.*, 2007). Throughout this manuscript, when making reference to the anthropogenic and contemporary CO₂ fluxes, we are specifically referring to fluxes from this second set of simulations (450 ppmv), unless otherwise stated.

In each set of simulations, we conduct one control run with constant physical forcing, one run with increasing wind stress, and another run with increasing freshwater flux from 1980 to 2100 (Table 1). Figures 2b and 2c show the beginning and ending profiles used for and derived from these perturbation runs. In our wind perturbation experiment, zonal wind is linearly interpolated from the solid to the dashed line over a 120-year period. The

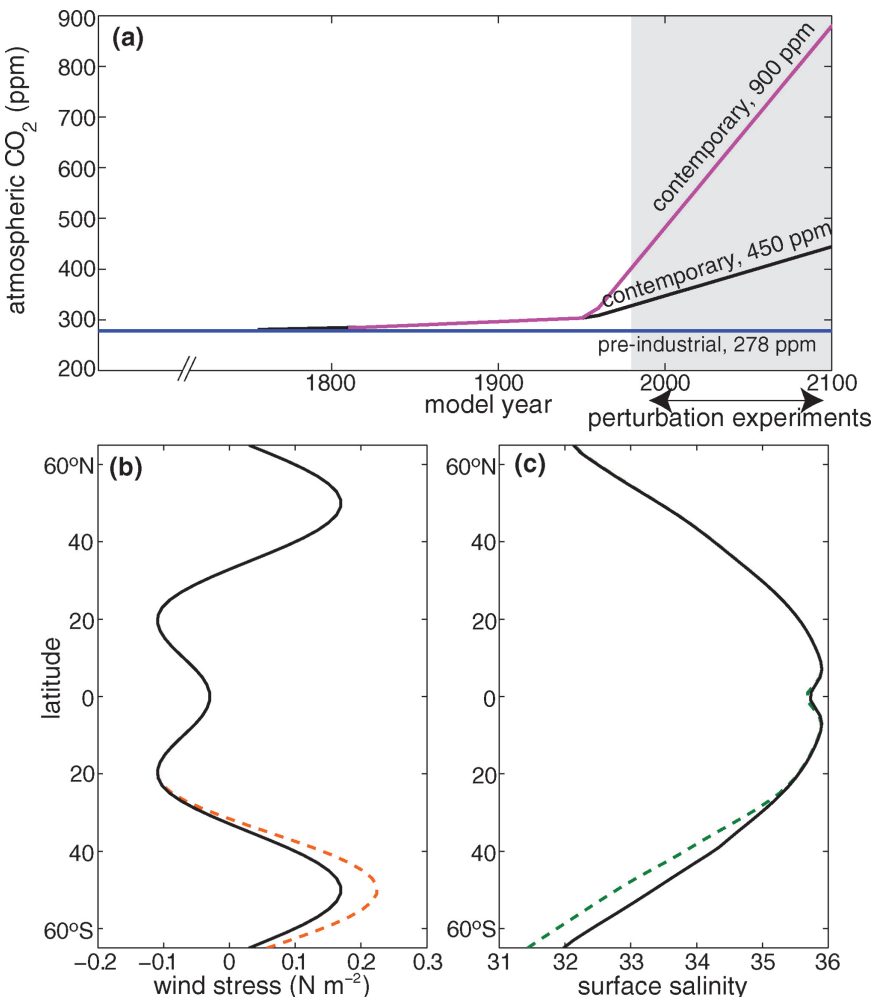


Figure 2. (a) Atmospheric $p\text{CO}_2$ (ppmv) boundary conditions used for the sensitivity experiments. (b) Wind stress (N m^{-2}) profiles used in the control and perturbation experiments, where the magnitude of the wind stress at 50°S was increased linearly from the control to the perturbed value over a 120-year period. (c) Zonal-mean surface salinity resulting from the control and freshwater perturbation experiments, where the Southern Ocean surface freshwater flux was increased linearly for a 120-year period.

magnitude of the wind stress perturbation was determined by extrapolating the approximate historical (1958–2004) trend in wind stress magnitude from the NCEP/NCAR reanalysis into the future. Note that the mean position of maximum wind stress does not change with time in this set of experiments. We conducted one additional experiment where the position of maximum wind stress moves poleward with time (Table 1). We mimic the effect of

Table 2. Southern Ocean stratification changes from the freshwater perturbation experiment with the sector model, and predicted stratification changes from the IPCC AR4 models (W. Lefebvre, pers. comm., 2008). Stratification calculated as the difference in potential density between 300 m and the surface, and change calculated as the difference between years 2091–2100 and 1991–2000 (kg m^{-3}).

Latitude	Sector model	IPCC AR4
30–40°S	−0.02	0.14
40–50°S	0.04	0.14
50–60°S	0.11	0.13
60–65°S	0.10	0.08

increased stratification by increasing the high latitude freshwater flux input with time. This imposed change in freshwater flux lowers the surface salinity (Fig. 2c) and causes the high latitude regions (<50°S) of the Southern Ocean to stratify nearly as much as predicted by the IPCC AR4 multi-model mean estimates in the year 2100 (Table 2). We purposely chose to force the system with freshwater flux boundary conditions rather than a uniformly imposed salinity to allow the model ocean to find weak points in stratification through which its ventilation can occur (Toggweiler and Bjornsson, 2000).

The model output is analyzed using spatial integration, spatial averages, and zonal-mean properties. Spatial integration and averaging is done over the entire Southern Ocean, in the region between 30°S and 65°S, while taking into account the relative area of each grid cell. Zonal averages of a property, however, are calculated simply as an arithmetic mean at each latitude, and are displayed without consideration for the area of that region.

3. Evaluation of the modeled mean state

Conducting idealized experiments with a simple ocean biogeochemical model helps to clarify the important mechanisms affecting air-sea CO_2 flux. However, it is necessary to first evaluate the sector model in its mean state to determine its strengths and weaknesses. Here, we compare output from the sector model with observations and a global ocean model with complex biogeochemical parameterizations. We limit our evaluation to zonal mean air-sea CO_2 fluxes, as the physical circulation has been previously described in a former version of the sector model (Ito and Follows, 2005).

Our simple model can capture broad patterns and magnitudes of the annual-mean (year 2000), zonal-mean contemporary CO_2 flux in the Southern Hemisphere, as compared to observations (Takahashi *et al.*, 2009) and simulations of the ECO-CCSM model (Lovenduski *et al.* (2007), Fig. 3a). Oceanic uptake of contemporary CO_2 occurs in the region between 20 and 50°S, where natural CO_2 uptake is strong (Fig. 3b), whereas we find the region south of 50°S to be neither a source nor sink of contemporary CO_2 , as the strong natural CO_2 outgassing is compensated by anthropogenic CO_2 uptake (Fig. 3b). The sector model underestimates the outgassing south of 60°S relative to the observations and forward ocean model; however, the ocean inversion model described in Gruber *et al.* (2009) predicts uptake of CO_2 in the region south of 58°S. Also, our simple sector model does not

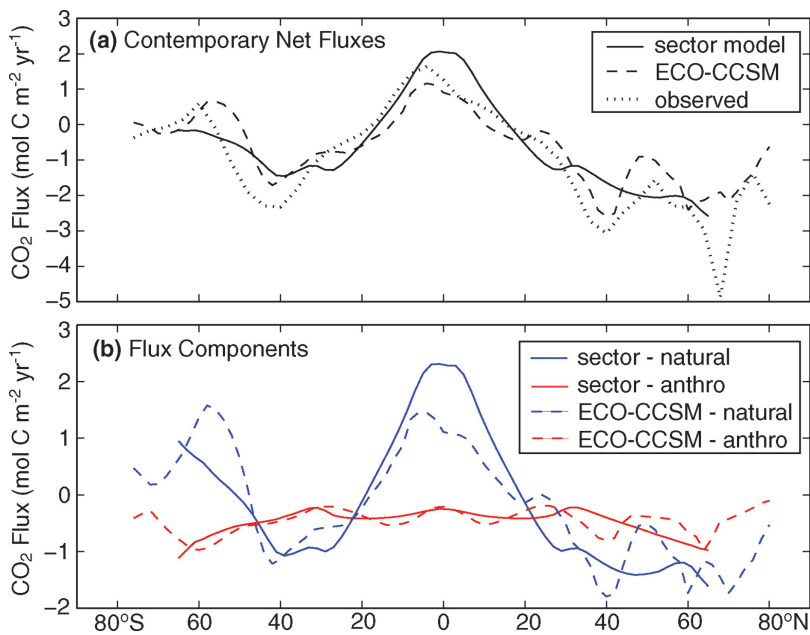


Figure 3. Annual-mean, zonal-mean (a) contemporary, (b) natural and anthropogenic CO_2 fluxes from the sector model (solid), global ECO-CCSM model (dashed), and the global CO_2 flux climatology of Takahashi *et al.* (2009) (dotted) in the year 2000. Positive fluxes denote ocean outgassing.

account for the freezing and melting of sea-ice, a process that may play an important role in controlling the $p\text{CO}_2$ budget in this high-latitude region (Metzl *et al.*, 2006). Both the sector and ECO-CCSM models underestimate the CO_2 uptake in the mid latitudes of the Southern Hemisphere.

The zonal-mean natural and anthropogenic CO_2 fluxes found in our sector model also agree remarkably well with fluxes estimated from the ECO-CCSM (Fig. 3b). The natural outgassing peak in the ECO-CCSM at 60°S is not found at the correct latitude in the sector model, perhaps due to the absence of sea ice and our idealized configuration of the model domain (Fig. 1).

The temporal evolution of the zonal-mean fluxes of natural, anthropogenic, and contemporary CO_2 from the control (constant physical forcing) runs is shown in the first row of Figure 4. Our model Southern Ocean is a source of natural CO_2 to the atmosphere in the region south of 50°, and a sink of natural CO_2 in the region north of this latitude. These patterns of natural CO_2 exchange do not change with time, owing to the fixed boundary condition for atmospheric $p\text{CO}_2$ in this run. Our model Southern Ocean is everywhere absorbing anthropogenic CO_2 from the atmosphere, with a higher uptake occurring in high latitudes and the region north of 30°S. Absorption of anthropogenic CO_2 is increasing with time in our model due to the prescribed increase in the atmospheric $p\text{CO}_2$ boundary condition. The contemporary fluxes of CO_2 are the sum of the natural and anthropogenic fluxes,

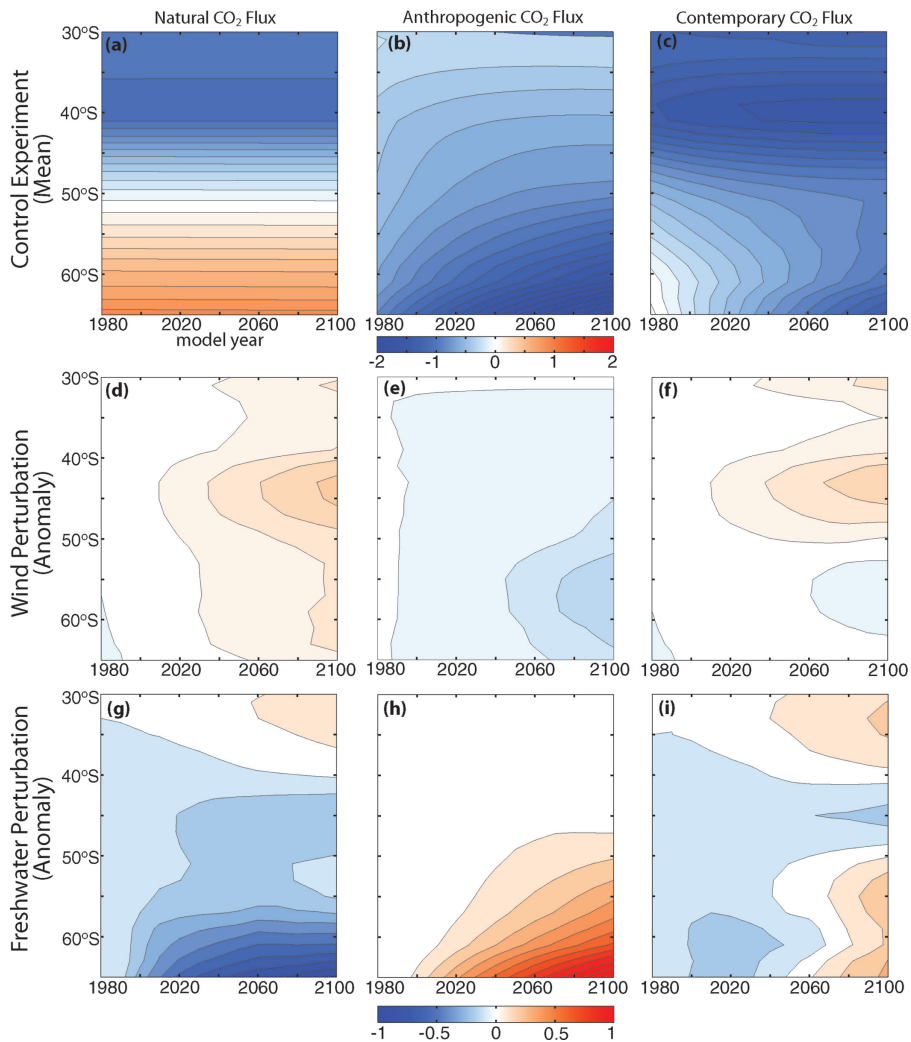


Figure 4. Temporal evolution of the zonal-mean fluxes of (1st column) natural, (2nd column) anthropogenic, and (3rd column) contemporary CO₂. (1st row) Control experiment plotted with contours every 0.1 mol m⁻² yr⁻¹. Anomalies in CO₂ flux from the (2nd row) wind perturbation and (3rd row) freshwater perturbation experiments plotted with contours every 0.05 mol m⁻² yr⁻¹. Positive fluxes indicate outgassing.

and as such, are somewhat difficult to interpret. Generally, our model Southern Ocean is a sink for total contemporary CO₂, and this sink strength is growing with time. The spatially-integrated Southern Ocean (<30°S) CO₂ fluxes exhibit this behavior as well (Fig. 5). We investigate in the following sections how these zonal and spatial mean fluxes evolve under increasing wind stress and increasing stratification.

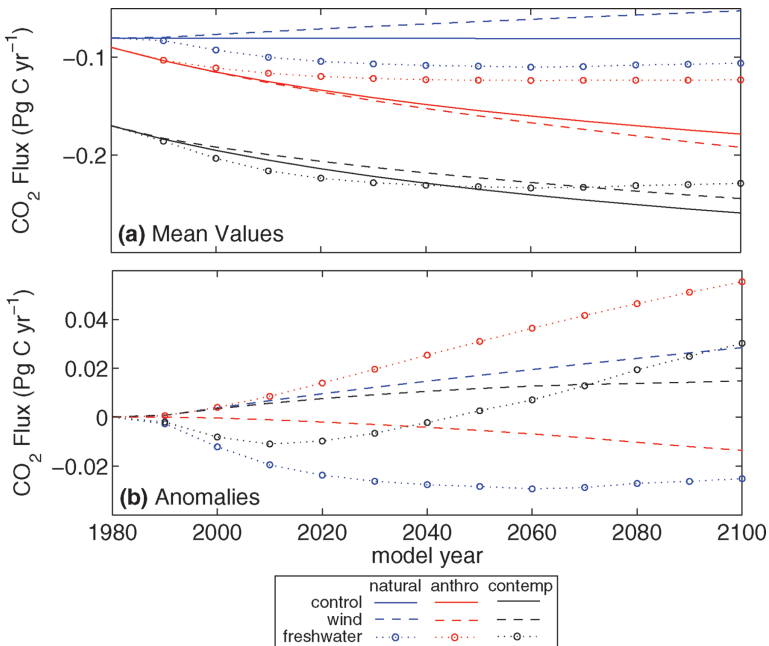


Figure 5. (a) Spatially-integrated Southern Ocean ($<30^{\circ}\text{S}$) flux of natural, anthropogenic, and total contemporary CO_2 during the control, wind perturbation, and freshwater perturbation experiments. (b) Southern Ocean CO_2 flux anomalies during the wind perturbation (wind minus control) and freshwater perturbation (freshwater minus control) experiments. Positive values denote (anomalous) outgassing. Note that the magnitude of the spatially-integrated fluxes cannot be directly compared with global ocean model output, due to the sector model's smaller domain size.

4. Wind perturbation

a. Natural CO_2 changes

The spatially-integrated ($<30^{\circ}\text{S}$) Southern Ocean sink of natural CO_2 weakens by about 50% of its control run value by 2100 in the wind perturbation experiment (Fig. 5a). The weaker sink under enhanced wind stress can also be expressed as a positive anomaly in natural CO_2 flux from this region (Fig. 5b). This anomalous outgassing is linearly increasing with time, as wind stress over the Southern Ocean is also linearly increasing. The spatial pattern of this anomalous natural CO_2 flux is shown in Figure 4d. Wind stress causes anomalous outgassing of natural CO_2 nearly everywhere in the Southern Ocean, but there is a concentrated region of outgassing between 40°S and 50°S , and at about 60°S .

We investigate the processes driving the anomalous outgassing of natural CO_2 under enhanced wind stress by decomposing the modeled air-sea CO_2 exchange, F_{CO_2} , into its contributing parameters (Lovenduski *et al.*, 2007),

$$F_{\text{CO}_2} = G(p\text{CO}_2^{\text{oc}} - p\text{CO}_2^{\text{atm}}),$$

Table 3. Estimated contributions to the change in natural ocean $p\text{CO}_2$, $\Delta p\text{CO}_2$, during the wind perturbation experiments, [μatm], averaged over the Southern Ocean ($<30^\circ\text{S}$). Σ is the sum of all five terms, and $\Delta p\text{CO}_{2,\text{mod}}$ is the modeled change in $p\text{CO}_2$.

year	$\frac{\partial p\text{CO}_2}{\partial s\text{DIC}} \Delta s\text{DIC}$	$\frac{\partial p\text{CO}_2}{\partial s\text{Alk}} \Delta s\text{Alk}$	$\frac{\partial p\text{CO}_2}{\partial f\text{w}} \Delta f\text{w}$	$\frac{\partial p\text{CO}_2}{\partial T} \Delta T$	$\frac{\partial p\text{CO}_2}{\partial S} \Delta S$	Σ	$\Delta p\text{CO}_{2,\text{mod}}$
<i>Wind Magnitude Perturbation</i>							
2000	0.89	-0.19	0	-0.03	0	0.66	0.58
2050	4.19	-1.20	-0.01	-0.11	-0.01	2.86	2.63
2100	7.27	-2.33	-0.02	-0.20	-0.02	4.70	4.36
<i>Wind Position Perturbation</i>							
2000	-0.04	0.01	0	0	0	-0.03	-0.02
2050	-0.50	0.12	0	0.02	0	-0.36	-0.31
2100	-1.06	0.27	0.01	0.04	0.01	-0.73	-0.68

where G is a measure of gas exchange (a function of gas transfer velocity, sea ice fraction, and solubility), $p\text{CO}_2^{\text{oc}}$ is the surface ocean $p\text{CO}_2$, and $p\text{CO}_2^{\text{atm}}$ is the $p\text{CO}_2$ of the overlying atmosphere. As G changes very little between our control and wind-perturbed experiments (constant gas transfer velocity and no sea ice fraction), and $p\text{CO}_2^{\text{atm}}$ is constant, the primary mechanism creating anomalies in the natural CO_2 fluxes under enhanced wind stress are anomalies in the ocean surface $p\text{CO}_2$, $\Delta p\text{CO}_2^{\text{oc}}$. We consider the total derivative for this quantity and its decomposition into contributions from DIC, alkalinity (Alk), temperature, and salinity,

$$\Delta p\text{CO}_2^{\text{oc}} = \frac{\partial p\text{CO}_2^{\text{oc}}}{\partial \text{DIC}} \Delta \text{DIC} + \frac{\partial p\text{CO}_2^{\text{oc}}}{\partial \text{Alk}} \Delta \text{Alk} + \frac{\partial p\text{CO}_2^{\text{oc}}}{\partial T} \Delta T + \frac{\partial p\text{CO}_2^{\text{oc}}}{\partial S} \Delta S, \quad (1)$$

where $\frac{\partial p\text{CO}_2^{\text{oc}}}{\partial \text{DIC}}$, $\frac{\partial p\text{CO}_2^{\text{oc}}}{\partial \text{Alk}}$, $\frac{\partial p\text{CO}_2^{\text{oc}}}{\partial T}$, and $\frac{\partial p\text{CO}_2^{\text{oc}}}{\partial S}$ are determined from the equations in Sarmiento and Gruber (2006) and the spatially averaged Southern Ocean values in the control simulation (see Appendix for more details). ΔDIC , ΔAlk , ΔT , and ΔS are the differences of the spatially-averaged Southern Ocean DIC, Alk, T, and S, respectively in the wind perturbed experiment and the control experiment.

Anomalies in DIC and Alk can be driven by changes in ocean transport/mixing and biological uptake/remineralization, but also by changes in freshwater fluxes (Δfw). We separate these two components of change by normalizing DIC and Alk with salinity ($s\text{DIC}$ and $s\text{Alk}$), and expanding our total $p\text{CO}_2^{\text{oc}}$ derivative (see Appendix for more details),

$$\begin{aligned} \Delta p\text{CO}_2^{\text{oc}} = & \frac{S}{S_0} \frac{\partial p\text{CO}_2^{\text{oc}}}{\partial \text{DIC}} \Delta s\text{DIC} + \frac{S}{S_0} \frac{\partial p\text{CO}_2^{\text{oc}}}{\partial \text{Alk}} \Delta s\text{Alk} \\ & + \frac{\partial p\text{CO}_2^{\text{oc}}}{\partial \text{fw}} \Delta \text{fw} + \frac{\partial p\text{CO}_2^{\text{oc}}}{\partial T} \Delta T + \frac{\partial p\text{CO}_2^{\text{oc}}}{\partial S} \Delta S, \end{aligned} \quad (2)$$

whose individual terms are shown in the top section of Table 3.

As the anomalous surface ocean $p\text{CO}_2$ under increased wind stress exhibits a linear behavior, we show the contributions to $\Delta p\text{CO}_2$ for three time slices (Table 3). In each

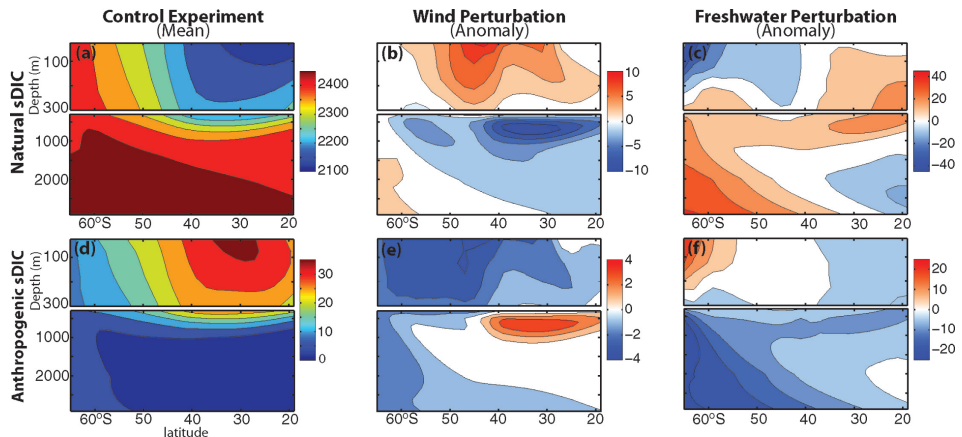


Figure 6. Zonal mean (1st row) natural and (2nd row) anthropogenic sDIC. (1st column) Annual mean sDIC during year 1980 of the control experiment is plotted alongside anomalies in sDIC during year 2100 from the (2nd column) wind perturbation and (3rd column) freshwater perturbation experiments. Units are mmol m^{-3} .

slice, it is clear that the primary driver for the positive anomalies in $p\text{CO}_2^{\text{oc}}$ is the large positive contribution from the sDIC term, which is being somewhat mitigated by the negative contribution from the sAlk term. Contributions from freshwater, T, and S play comparatively smaller roles.

sDIC is an important constituent of the total $p\text{CO}_2$ anomaly budget because its surface distribution is linearly increasing with time in the wind perturbation experiment (Fig. 6b). The surface increase is largest in the region between 40°S and 50°S, where wind stress drives anomalous advection of natural DIC via increased upwelling and northward Ekman transport (Fig. 6a, Fig. 7). The linear increase in sDIC, and thus $p\text{CO}_2^{\text{oc}}$ is driven by the linear change in the overturning circulation, which is responding to the increased wind stress. Ultimately, this process causes a linear decrease in the strength of the Southern Ocean sink for natural CO_2 (Fig. 5). The decreasing sink strength is most prominent in the regions of anomalous upwelling ($\sim 60^\circ\text{S}$) and anomalous Ekman transport ($\sim 45^\circ\text{S}$, Fig. 4d), where the surface distribution of sDIC is changing the most.

b. Anthropogenic CO_2 changes

Our model Southern Ocean sink for anthropogenic CO_2 strengthens by 0.01 Pg C yr⁻¹ in 2100 under increasing wind stress and with atmospheric CO_2 stabilization at 450 ppmv (Fig. 5a). This strengthening sink can also be expressed as a negative anomaly in anthropogenic CO_2 exchange, which exhibits a linear behavior with time (Fig. 5b). The anomalous uptake is found nearly everywhere in the Southern Ocean, but is highest in the region just north of 60°S during the final 50 years of the experiment (Fig. 4e).

The changes in meridional overturning brought on by the increasing wind stress (Fig. 7) cause large changes in the distribution of anthropogenic sDIC in our model. Anthropogenic

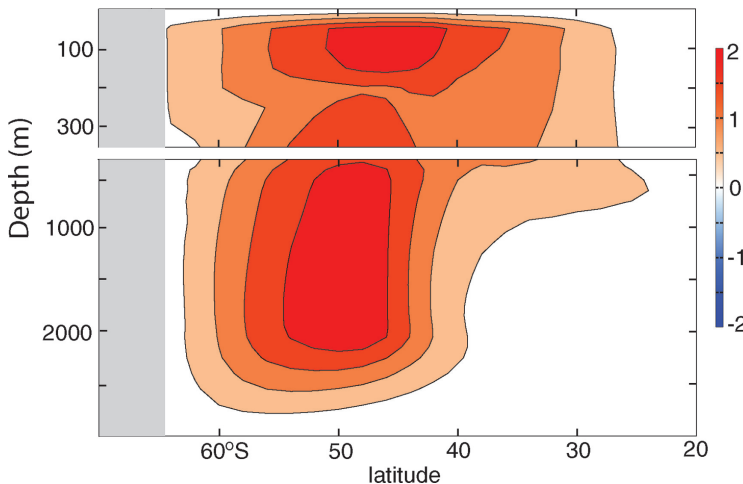


Figure 7. Anomaly in residual-mean (eulerian + bolus) meridional overturning streamfunction during the wind perturbation experiment, year 2100. Contours are every 0.5 Sv.

sDIC has a mean distribution that is higher at the surface than at depth (Fig. 6d). When increased wind drives enhanced upwelling in the high latitude regions, there is an anomalous increase in the supply of waters low in anthropogenic sDIC to the surface. This supply lowers the surface concentration of anthropogenic sDIC (Fig. 6e) and allows the ocean to absorb more anthropogenic CO₂ from the atmosphere. The anthropogenic CO₂ fluxes do not respond as dramatically to changes in wind stress as the natural CO₂ fluxes, as the mean horizontal and vertical gradients in anthropogenic sDIC are much smaller than those of natural sDIC (compare Figs. 6a and d).

Increasing wind stress, then, allows the Southern Ocean to absorb slightly more anthropogenic CO₂ than it would with constant wind, due to enhanced upwelling of waters low in anthropogenic CO₂ and faster exposure of these waters to the atmosphere. These results are in agreement with the study by Russell *et al.* (2006). When the same wind stress increase acts on a larger gradient in air-sea *p*CO₂, however, the magnitude of the changes in anthropogenic CO₂ uptake can be even larger. This is shown in Figure 8, where the experiments were run with a more rapid increase in the atmospheric *p*CO₂ boundary condition, so that it reached 900 ppmv by 2100. The relative increase in anthropogenic CO₂ uptake under enhanced wind stress in this case is 0.04 Pg C yr⁻¹ by 2100, approximately four times the increase in the 450 ppmv simulation.

c. Contemporary CO₂ changes

Overall, we find the Southern Ocean to be a weaker sink for total contemporary CO₂ by the year 2100 in our wind perturbation experiment (Fig. 5a). This is because the natural CO₂ outgassing anomaly is growing with time at a faster rate than the anthropogenic CO₂

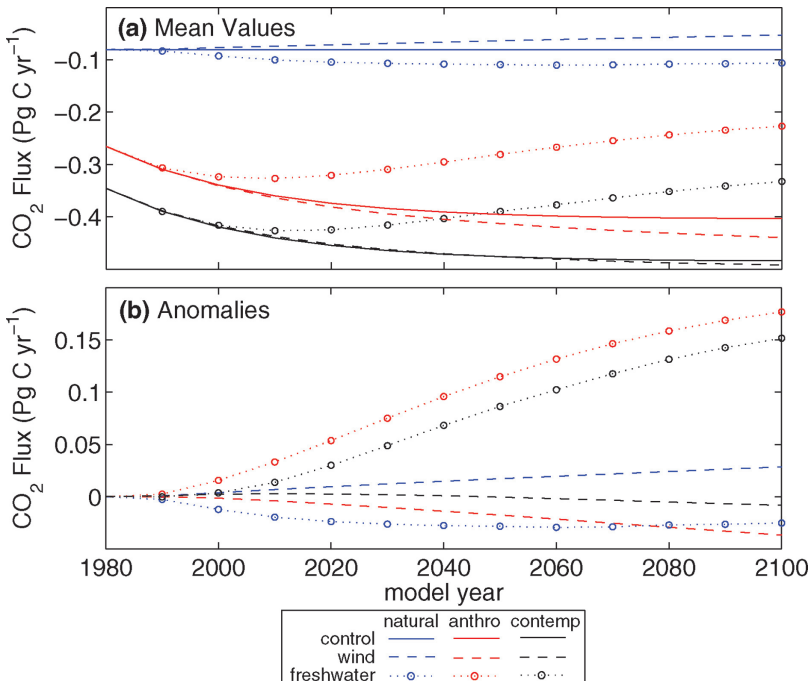


Figure 8. Same as Figure 5, except for the simulations where the boundary condition for atmospheric $p\text{CO}_2$ reaches 900 ppmv by 2100.

uptake anomaly, so the net effect is an anomaly toward outgassing of total contemporary CO_2 by 2100 (Fig. 4f, Fig. 5b).

Using simple box models and coupled general circulation models, several authors (Zickfeld *et al.*, 2007; Le Quéré *et al.*, 2008; Matear and Lenton, 2008) have hypothesized that the coming century will be characterized by a reversal of this contemporary CO_2 sink anomaly. They suggest that increasing wind stress, coupled with the predicted rise in atmospheric CO_2 will act to first weaken, then strengthen the Southern Ocean sink for contemporary CO_2 . While we do not observe this behavior when our atmospheric $p\text{CO}_2$ boundary condition reaches 450 ppmv by 2100 (Fig. 5), our model does exhibit this behavior when this boundary condition rises to 900 ppmv by 2100 (Fig. 8). In this case, natural CO_2 uptake continues to weaken under enhanced wind stress, but anthropogenic CO_2 uptake strengthens at a faster rate, causing a reversal in the net contemporary CO_2 flux anomaly at ~ 2050 . Thus, our results are sensitive to the atmospheric $p\text{CO}_2$ boundary condition used in our simulations.

d. Wind position perturbation

In order to separately examine the relative importance of wind magnitude and position changes, we conduct an additional experiment where the magnitude of the maximum wind

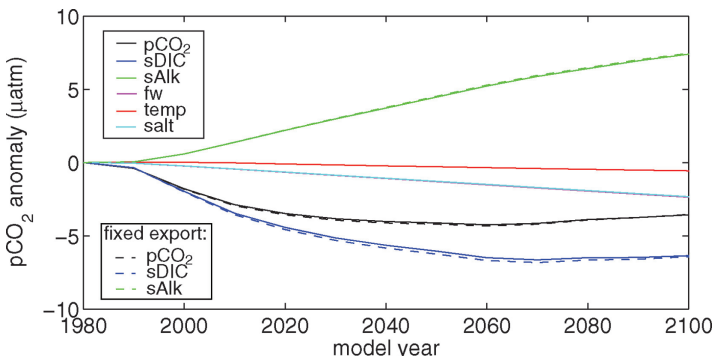


Figure 9. Temporal evolution of the anomaly in mean natural $p\text{CO}_2$ from the surface of the Southern Ocean ($\Delta p\text{CO}_2^{\text{oc}}$; black), and the components contributing to this anomaly (colors) during the freshwater perturbation experiment as in equation (2). Units are μatm . Results from a freshwater perturbation experiment with fixed biological export are shown as dashed lines.

stress remains constant, but its position moves poleward by 0.75° over 120 years (Table 1). Moving the maximum wind stress reduces the surface ocean $p\text{CO}_2$ by a small amount, primarily as a consequence of lower DIC in the surface waters (Table 3). This wind movement is accompanied by a 0.005 kg m^{-3} reduction in high latitude surface density, which decreases the size of the outcrop area for DIC-rich waters (Tschumi *et al.*, 2008), and lowers the natural CO_2 outgassing from this region. While the sign of this change in natural CO_2 flux is opposite to that of the wind strength perturbation experiment (Section 4a), its magnitude is much smaller.

5. Freshwater perturbation

a. Natural CO_2 changes

The spatially-integrated Southern Ocean sink for natural CO_2 strengthens in the freshwater perturbation simulation, as compared to the control run (Fig. 5a). This negative anomaly in natural CO_2 flux is evident everywhere in the Southern Ocean, but is concentrated in the high latitude regions (Fig. 4g). A linear change in freshwater supply causes a non-linear change in the integrated flux anomalies with time (Fig. 5b). At first, increased freshwater causes the sink strength to increase dramatically, but this behavior does not continue beyond 2060, where the anomalous time series stops decreasing and begins to slightly increase.

We investigate the processes responsible for the behavior of the freshwater perturbation anomalies in natural CO_2 using the technique described in Section 4a. We decompose the anomaly in surface ocean $p\text{CO}_2$, $\Delta p\text{CO}_2$ into the components contributing to change at each time step and display the results in Figure 9. This analysis reveals that anomalies in surface ocean $p\text{CO}_2$ are primarily a result of contributions from the sDIC term, with the sAlk term slightly mitigating the response. As was the case for increasing wind

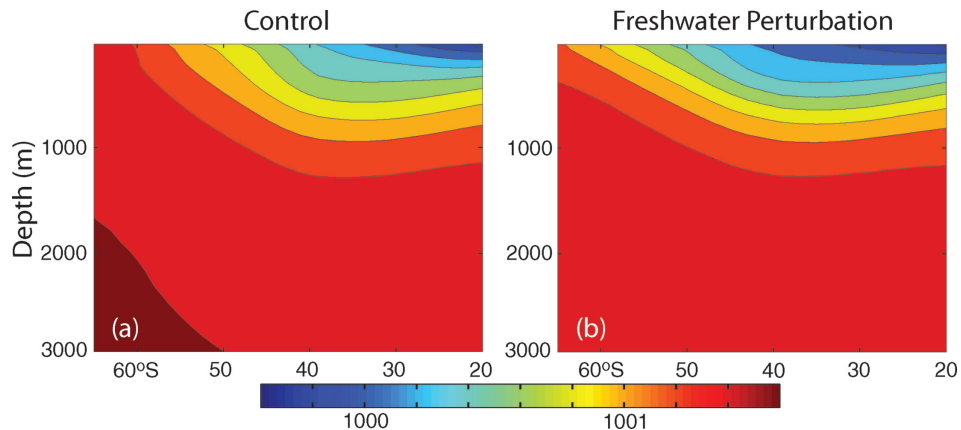


Figure 10. Annual-mean, zonal-mean potential density in the (a) control and (b) freshwater perturbation experiments in the year 2100. Contour intervals are 0.2 kg m^{-3} .

stress, changes in freshwater, T, and S play comparatively smaller roles in the overall budget.

Adding freshwater to the Southern Ocean decreases surface density, resulting in dramatic changes in stratification (Fig. 10). Increased stratification causes the isopycnal surfaces to flatten, reducing the outcrop area for upwelling water and changing the entire surface and interior ocean distribution of natural sDIC (Fig. 6c). The result is a surface ocean characterized by much lower sDIC, and therefore $p\text{CO}_2$, and an accumulation of sDIC in the deep parts of the high latitudes. Stratification also lowers surface ocean sAlk, although its effect on $p\text{CO}_2$ is smaller.

The non-linearity in the surface ocean $p\text{CO}_2$ anomaly is closely tied with the non-linear behavior in the surface ocean sDIC. This behavior appears a result of the slow flattening of the isopycnal surfaces under increased freshwater forcing (Fig. 10), which changes the characteristics of the upwelling/outcropping water in the high-latitudes. After a certain time (~ 2060 in our simulation), the deep water enriched in sDIC is prevented from reaching the surface and continued flattening of isopycnals has no impact on surface sDIC concentrations.

Increased stratification also has an impact on nutrient supply and biological production in our model, although its impact on the air-sea CO_2 flux is only a small component of change. Fig. 9 (dashed lines) shows the $\Delta p\text{CO}_2$ budget results from an identical freshwater simulation, but one where export production was fixed, rather than evolving with surface phosphate concentration. A visual comparison of these time series with the ones from the original simulation indicates that the increase in stratification slowly decreased the supply of phosphate to the surface ocean, and slowed the biological drawdown of DIC and Alk. However, the overall influence of this biological slow-down is of little consequence for the total natural $p\text{CO}_2^{\text{oc}}$ budget.

b. Anthropogenic CO₂ changes

The Southern Ocean sink for anthropogenic CO₂ weakens considerably in our freshwater perturbation experiment, relative to the control experiment (Fig. 5a). This results in positive anthropogenic CO₂ flux anomalies which exhibit a non-linear behavior with time (Fig. 5b). The anomalies are concentrated in the high latitude regions of the Southern Ocean (Fig. 4h).

The increased stratification brought on by increases in surface freshwater slows the upwelling of waters depleted in anthropogenic sDIC (Fig. 6d, 6f), reducing the ability of the surface ocean to absorb anthropogenic CO₂ from the atmosphere. This result is consistent with that of Sarmiento *et al.* (1998), who find that century-scale changes in stratification reduce the downward flux of anthropogenic carbon in the Southern Ocean.

The stratification-imposed weakening of the Southern Ocean sink for anthropogenic CO₂ is amplified as the ocean-atmosphere gradient in *p*CO₂ increases. Figure 8 shows the anthropogenic CO₂ flux response to the same stratification increase in a simulation where the atmospheric boundary condition for *p*CO₂ grows to 900 ppmv by 2100. The anomalous response to stratification is even more dramatic in this case, with the anthropogenic CO₂ sink weakening to about 50% of its value in the control run by 2100.

c. Contemporary CO₂ changes

The non-linear response of natural and anthropogenic CO₂ flux to increased freshwater supply causes the total sink for contemporary CO₂ to first strengthen, then weaken, as compared to the control simulation (Fig. 4i, 5). At the beginning of the freshwater perturbation simulation, anomalies in natural CO₂ uptake dominate the anomalies in anthropogenic CO₂ outgassing, but after ~2040, the anthropogenic CO₂ outgassing anomalies begin to dominate, and the net response is reversed. While enhanced stratification may increase the drawdown of atmospheric CO₂ at first, by 2100, our simulation suggests that the Southern Ocean will become a weaker sink for total contemporary CO₂.

Increasing atmospheric CO₂ amplifies the weakening of the anthropogenic CO₂ flux in response to higher stratification, overwhelming the anomalous natural CO₂ uptake, and causing the Southern Ocean sink for contemporary CO₂ to weaken throughout the course of the simulation, as compared to the control run (Fig. 8). This implies that a future characterized by increased Southern Ocean stratification and rapidly increasing atmospheric CO₂ concentrations will also be characterized by a weakening Southern Ocean CO₂ sink.

6. Simultaneous wind and freshwater perturbations

We have demonstrated that increasing wind and increasing stratification separately lead to large changes in the Southern Ocean sink for contemporary CO₂ by 2100, through a complex interaction of the circulation with natural and anthropogenic CO₂. It is worth contemplating, then, how a future characterized by both increased wind stress and increased stratification will impact the Southern Ocean CO₂ sink. Figure 11 shows results from two sets of experiments where both wind stress and freshwater forcing linearly increase with

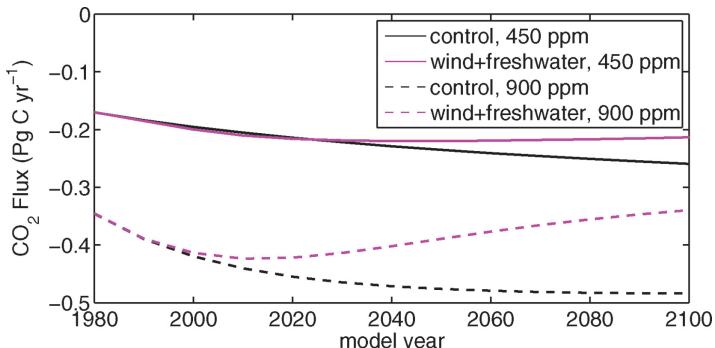


Figure 11. Spatially-integrated Southern Ocean ($<30^{\circ}$ S) fluxes of contemporary CO₂ from control experiments with no change in physical forcing (black) and from experiments where wind stress and freshwater fluxes simultaneously increase with time (magenta). Differing boundary conditions for atmospheric $p\text{CO}_2$ were used in the experiments: 450 ppmv (solid), and 900 ppmv (dashed) by 2100 (see Figure 2a).

time. In the first (second) set, the atmospheric $p\text{CO}_2$ boundary condition increases to 450 (900) ppmv by 2100. Both sets of simulations indicate that the Southern Ocean sink for total contemporary CO₂ will be weaker under simultaneous increases in wind stress and stratification, as compared to control simulations with no changes in physical forcing. The net response of the CO₂ fluxes to these simultaneous changes is essentially a linear superposition of the responses to the individual changes. Simultaneous changes in wind and stratification are likely to occur in the future, as shifts in the position and intensity of wind stress and precipitation are naturally correlated in the storm track.

7. Discussion and conclusions

We conclude that the Southern Ocean CO₂ sink is very sensitive to changes in wind stress and stratification. A linear increase in wind stress drives a linear decrease in contemporary CO₂ uptake, as anomalies in natural CO₂ outgassing overwhelm enhanced anthropogenic CO₂ uptake. These anomalies are caused by changes in the upwelling and northward surface transport of DIC. Wind-induced changes in anthropogenic CO₂ are sensitive to the atmospheric $p\text{CO}_2$ boundary condition. A poleward shift in the wind stress reduces the high-latitude isopycnal outcrop area and slightly decreases natural CO₂ outgassing. We find that a linear increase in freshwater forcing leads to first an increase, then a decrease in contemporary CO₂ uptake, caused by a complex interaction of the non-linear natural and anthropogenic CO₂ anomalies. Increased stratification causes a shift in the location of isopycnal outcrop, creating changes in the DIC distribution. Simultaneous increases in wind stress and stratification lead to a weaker sink for atmospheric CO₂ in the Southern Ocean by 2100.

Our simple approach to providing a mechanistic understanding of the CO₂ flux changes with changes in wind stress and stratification does not come without caveats. The coarse resolution of our model domain does not permit eddy-scale interactions to occur, and their effects must be parameterized. Recent literature highlights the importance of these eddies in controlling the long-term circulation response to wind stress (Böning *et al.*, 2008), and the mean anthropogenic CO₂ transport in the Southern Ocean (Ito *et al.*, 2010). Also, our results de-emphasize the role of biological uptake in controlling the CO₂ flux response in the Southern Ocean, in contrast to idealized simulations on millennial timescales (Tschumi *et al.*, 2008). Restricting our analysis to the Southern Ocean and to short time scales precludes us from investigation of the global biological response to the slow change in thermocline nutrients that may originate in the Southern Ocean (Sarmiento *et al.*, 2004a; Dutkiewicz *et al.*, 2005).

Despite these caveats, and the somewhat unrealistic formulation of our model and perturbation experiments, results from our idealized experiments highlight the potential for the Southern Ocean to experience large changes in the coming century, and argue strongly for improved observational effort in this region.

Acknowledgments. NSL was supported by the NOAA Climate and Global Change Postdoctoral Research Fellowship, and TI was supported by NASA NNX08AL72G. We thank W. Lefebvre and H. Goosse for giving us access to their Southern Ocean stratification data and for discussing their analysis with us.

APPENDIX

pCO₂^{oc} partial derivatives

Anomalies in surface ocean *pCO₂* during the perturbation experiments, ($\Delta p\text{CO}_2^{\text{oc}}$) are decomposed into the contributions from DIC, Alk, T, and S according to (1). We use the following set of equations to approximate the Southern Ocean (<30°S) mean values of the *pCO₂^{oc}* partial derivatives (Sarmiento and Gruber, 2006),

$$\frac{\partial p\text{CO}_2^{\text{oc}}}{\partial \text{DIC}} = \frac{p\text{CO}_2^{\text{oc}}}{\text{DIC}} \times \gamma_{\text{DIC}}$$

$$\frac{\partial p\text{CO}_2^{\text{oc}}}{\partial \text{Alk}} = \frac{p\text{CO}_2^{\text{oc}}}{\text{Alk}} \times \gamma_{\text{Alk}}$$

$$\frac{\partial p\text{CO}_2^{\text{oc}}}{\partial \text{T}} \approx p\text{CO}_2^{\text{oc}} \times 0.0423^{\circ}\text{C}^{-1}$$

$$\frac{\partial p\text{CO}_2^{\text{oc}}}{\partial \text{S}} \approx \frac{p\text{CO}_2^{\text{oc}}}{\text{S}},$$

where the buffer factors can be approximated with

$$\gamma_{\text{DIC}} \approx \frac{3\text{Alk} \cdot \text{DIC} - 2\text{DIC}^2}{(2\text{DIC} - \text{Alk})(\text{Alk} - \text{DIC})}$$

$$\gamma_{\text{Alk}} \approx -\frac{\text{Alk}^2}{(2\text{DIC} - \text{Alk})(\text{Alk} - \text{DIC})}.$$

Salinity normalization

To separate the contribution from freshwater fluxes on DIC and Alk, we use the following two equations for the first and second terms of (1),

$$\begin{aligned} \frac{\partial p\text{CO}_2^{\text{oc}}}{\partial \text{DIC}} \Delta \text{DIC} &= \frac{\partial p\text{CO}_2^{\text{oc}}}{\partial (\text{S}/\text{S}_0 \text{sDIC})} \Delta (\text{S}/\text{S}_0 \text{sDIC}) \\ &= \frac{\text{sDIC}}{\text{S}_0} \frac{\partial p\text{CO}_2^{\text{oc}}}{\partial \text{DIC}} \Delta \text{S} + \frac{\text{S}}{\text{S}_0} \frac{\partial p\text{CO}_2^{\text{oc}}}{\partial \text{DIC}} \Delta \text{sDIC} \\ \frac{\partial p\text{CO}_2^{\text{oc}}}{\partial \text{Alk}} \Delta \text{Alk} &= \frac{\partial p\text{CO}_2^{\text{oc}}}{\partial (\text{S}/\text{S}_0 \text{sAlk})} \Delta (\text{S}/\text{S}_0 \text{sAlk}) \\ &= \frac{\text{sAlk}}{\text{S}_0} \frac{\partial p\text{CO}_2^{\text{oc}}}{\partial \text{Alk}} \Delta \text{S} + \frac{\text{S}}{\text{S}_0} \frac{\partial p\text{CO}_2^{\text{oc}}}{\partial \text{Alk}} \Delta \text{sAlk}. \end{aligned}$$

We extract the first terms from the above two equations, as they represent the contribution from freshwater forcing (fw) on $p\text{CO}_2^{\text{oc}}$,

$$\frac{\partial p\text{CO}_2^{\text{oc}}}{\partial \text{fw}} \Delta \text{fw} = \frac{\text{sDIC}}{\text{S}_0} \frac{\partial p\text{CO}_2^{\text{oc}}}{\partial \text{DIC}} \Delta \text{S} + \frac{\text{sAlk}}{\text{S}_0} \frac{\partial p\text{CO}_2^{\text{oc}}}{\partial \text{Alk}} \Delta \text{S}.$$

REFERENCES

- Bitz, C. M., P. R. Gent, R. A. Woodgate, M. M. Holland and R. Lindsay. 2006. The influence of sea ice on ocean heat uptake in response to increasing CO₂. *J. Climate*, *19*, 2437–2450.
- Böning, C. W., A. Dispert, M. Visbeck, S. R. Rintoul and F. U. Schwarzkopf. 2008. The response of the Antarctic Circumpolar Current to recent climate change. *Nature Geosci.*, *1*, 864–869, doi:[10.1038/ngeo336](https://doi.org/10.1038/ngeo336).
- Dutkiewicz, S., M. J. Follows and P. Parekh. 2005. Interactions of the iron and phosphorus cycles: A three-dimensional model study. *Global Biogeochem. Cycles*, *19*, GB1021, doi:[10.1029/2004GB002342](https://doi.org/10.1029/2004GB002342).
- Fung, I., S. C. Doney, K. Lindsay and J. John. 2005. Evolution of carbon sinks in a changing climate. *Proc. Nat. Acad. Sci.*, *102*, 11201–11206, doi:[10.1073/pnas.0504949102](https://doi.org/10.1073/pnas.0504949102).
- Gent, P. R. and J. C. McWilliams. 1990. Isopycnal mixing in ocean circulation models. *J. Phys. Oceanogr.*, *20*, 150–155.
- Gruber, N., M. Gloor, S. E. M. Fletcher, S. C. Doney, S. Dutkiewicz, M. J. Follows, M. Gerber, A. R. Jacobson, F. Joos, K. Lindsay, D. Menemenlis, A. Mouchet, S. A. Muller, J. L. Sarmiento and T. Takahashi. 2009. Oceanic sources, sinks, and transport of atmospheric CO₂. *Global Biogeochem. Cycles*, *23*, GB1005, doi:[10.1029/2008GB003349](https://doi.org/10.1029/2008GB003349).

- Hirst, A. C. 1999. The Southern Ocean response to global warming in the CSIRO coupled ocean-atmosphere model. *Env. Model. Software*, *14*, 227–241.
- Ito, T. and M. J. Follows. 2005. Preformed phosphate, soft tissue pump and atmospheric CO₂. *J. Mar. Res.*, *63*, 813–839.
- Ito, T., M. Woloszyn and M. Mazloff. 2010. Anthropogenic carbon dioxide transport in the Southern Ocean driven by Eckman Flow. *Nature*, *463*, doi:10.1038/nature08687.
- Le Quéré, C., C. Rödenbeck, E. T. Buitenhuis, T. J. Conway, R. Langenfelds, A. Gomez, C. Labuschagne, M. Ramonet, T. Nakazawa, N. Metzl, N. Gillett and M. Heimann. 2007. Saturation of the Southern Ocean CO₂ sink due to recent climate change. *Science*, *316*, 1735–1738, doi:10.1126/science.1136188.
- . 2008. Response to comments on “Saturation of the Southern Ocean CO₂ sink due to recent climate change.” *Science*, *319*, 570c, doi:10.1126/science.1147315.
- Lovenduski, N. S., N. Gruber and S. C. Doney. 2008. Toward a mechanistic understanding of the decadal trends in the Southern Ocean carbon sink. *Global Biogeochem. Cycles*, *22*, GB3016, doi:10.1029/2007GB003139.
- Lovenduski, N. S., N. Gruber, S. C. Doney and I. D. Lima. 2007. Enhanced CO₂ outgassing in the Southern Ocean from a positive phase of the Southern Annular Mode. *Global Biogeochem. Cycles*, *21*, GB2026, doi:10.1029/2006GB002900.
- Manabe, S. and R. J. Stouffer. 1993. Century-scale effects of increased atmospheric CO₂ on the ocean-atmosphere system. *Nature*, *364*, 215–218.
- Matear, R. J. and A. Lenton. 2008. Impact of historical climate change on the Southern Ocean carbon cycle. *J. Climate*, *21*, 5820–5834, doi:10.1175/2008JCLI2194.1.
- Meehl, G. A., T. G. Stocker, W. D. Collins, P. Friedlingstein, A. T. Gaye, J. M. Gregory, A. Kitoh, R. Knutti, J. M. Murphy, A. Noda, S. C. B. Raper, I. G. Watterson, A. J. Weaver and Z.-C. Zhao. 2007. Global climate projections, in *Climate Change 2007: The Physical Science Basis. Contribution of working group I to the Fourth Assessment Report of the Intergovernmental Panel on Climate Change*, S. Solomon *et al.*, eds., Cambridge University Press, 747–845.
- Metzl, N. 2009. Decadal increase of oceanic carbon dioxide in Southern Indian Ocean surface waters (1991–2007). *Deep-Sea Res. II*, *56*, 609–619.
- Metzl, N., C. Brunet, A. Jabaud-Jan, A. Poisson and B. Schauer. 2006. Summer and winter air-sea CO₂ fluxes in the Southern Ocean. *Deep-Sea Res. I*, *53*, 1548–1563, doi:10.1016/j.dsr.2006.07.006.
- Miller, R. L., G. A. Schmidt and D. T. Shindell. 2006. Forced annular variations in the 20th century Intergovernmental Panel on Climate Change Fourth Assessment Report models. *J. Geophys. Res.*, *111*, D18101, doi:10.1029/2005JD006323.
- Russell, J. L., K. W. Dixon, A. Gnanadesikan, R. J. Stouffer and J. R. Toggweiler. 2006. The Southern Hemisphere westerlies in a warming world: Propping open the door to the deep ocean. *J. Climate*, *19*, 6382–6390.
- Sarmiento, J. L. and N. Gruber. 2006. *Ocean Biogeochemical Dynamics*. Princeton University Press, Princeton, NJ, 526 pp.
- Sarmiento, J. L., N. Gruber, M. A. Brzezinski and J. P. Dunne. 2004a. High-latitude controls of thermocline nutrients and low latitude biological productivity. *Nature*, *427*, 56–60.
- Sarmiento, J. L., T. M. C. Hughes, R. J. Stouffer and S. Manabe. 1998. Simulated response of the ocean carbon cycle to anthropogenic climate warming. *Nature*, *393*, 245–249.
- Sarmiento, J. L., R. Slater, R. Barber, L. Bopp, S. C. Doney, A. C. Hirst, J. Kleypas, R. Matear, U. Mikolajewicz, P. Monfray, V. Soldatov, S. A. Spall and R. Stouffer. 2004b. Response of ocean ecosystems to climate warming. *Global Biogeochem. Cycles*, *18*, GB3003, doi:10.1029/2003GB002134.

- Takahashi, T., S. C. Sutherland, R. Wanninkhof, C. Sweeney, R. A. Feely, D. W. Chipman, B. Hales, G. Friedrich, F. Chavez, C. Sabine, A. Watson, D. C. E. Bakker, U. Schuster, N. Metzl, H. Yoshikawa-Inoue, M. Ishii, T. Midorikawa, Y. Nojiri, A. Kortzinger and T. Steinhoff. 2009. Climatological mean and decadal change in surface ocean pCO₂, and net sea-air CO₂ flux over the global oceans. *Deep-Sea Res. II*, **56**, 554–577.
- Toggweiler, J. R. 1999. Variation of atmospheric CO₂ by ventilation of the ocean's deepest water. *Paleoceanography*, **14**(5), 571–588.
- Toggweiler, J. R. and H. Bjornsson. 2000. Drake Passage and palaeoclimate. *J. Quater. Sci.*, **15**, 319–328.
- Tschumi, T., F. Joos and P. Parekh. 2008. How important are Southern Hemisphere wind changes for low glacial carbon dioxide? A model study. *Paleoceanography*, **23**, PA4208, doi:[10.1029/2008PA001592](https://doi.org/10.1029/2008PA001592).
- Wanninkhof, R. 1992. Relationship between wind speed and gas exchange over the ocean. *J. Geophys. Res.*, **97**, 7373–7382.
- Zickfeld, K., J. C. Fyfe, O. A. Saenko, M. Eby and A. J. Weaver. 2007. Response of the global carbon cycle to human-induced changes in Southern Hemisphere winds. *Geophys. Res. Lett.*, **34**, GL12712, doi:[10.1029/2006GL028797](https://doi.org/10.1029/2006GL028797).

Received: 12 December, 2008; revised: 24 July, 2009.